Wiener–Hopf Solution for Impenetrable Wedges at Skew Incidence

Vito G. Daniele and Guido Lombardi, *Member, IEEE*

***Abstract*—A new Wiener–Hopf approach for the solution of impenetrable wedges at skew incidence is presented. Mathematical aspects are described in a unified and consistent theory for angular region problems. Solutions are obtained using analytical and numerical-analytical approaches. Several numerical tests from the scientific literature validate the new technique, and new solutions for anisotropic surface impedance wedges are solved at skew incidence. The solutions are presented considering the geometrical and uniform theory of diffraction coefficients, total fields, and possible surface wave contributions.**

***Index Terms*—Diffraction, electromagnetic diffraction, electromagnetic surface waves, Fredholm integral equations, geometrical theory of diffraction (GTD), uniform theory of diffraction (UTD), wedges, Wiener–Hopf method.**

I. Introduction

ANALYTICAL methods nowadays are able to deal with diffraction problems involving wedges. However, a general solution of this problem for an impenetrable wedge at skew incidence is not completely available yet.

This paper examines the problem of the diffraction by a plane wave at skew incidence on an impenetrable wedge immersed in an homogeneous material with permittivity ε and permeability μ; see Fig. 1.

We consider only time harmonic electromagnetic fields with a time dependence specified by the factor $e^{j\omega t}$, which is omitted. The incident field is constituted by plane waves having the following longitudinal components:

$$\begin{cases} E_z^i = E_o e^{j\tau_o \rho \cos(\varphi-\varphi_o)} e^{-j\alpha_o z} \\ H_z^i = H_o e^{j\tau_o \rho \cos(\varphi-\varphi_o)} e^{-j\alpha_o z} \end{cases} \tag{1}$$

where β and φ_o are the zenithal and the azimuthal angles which define the direction of the plane wave $\hat{n}_i$: $k = \omega\sqrt{\mu\varepsilon}$, $\alpha_o = k\cos\beta$, $\tau_o = k\sin\beta$. Boundary conditions are applied on the two faces of the wedge (face a $\varphi = +\Phi$ and face b $\varphi = -\Phi$) and the tangential components of fields are related through the Leontovich conditions

$$\begin{aligned} \begin{bmatrix} E_z(\rho,\Phi) \\ E_\rho(\rho,\Phi) \end{bmatrix} &= \mathbf{Z_a} \begin{bmatrix} H_\rho(\rho,\Phi) \\ -H_z(\rho,\Phi) \end{bmatrix} \\ \begin{bmatrix} E_z(\rho,-\Phi) \\ E_\rho(\rho,-\Phi) \end{bmatrix} &= -\mathbf{Z_b} \begin{bmatrix} H_\rho(\rho,-\Phi) \\ -H_z(\rho,-\Phi) \end{bmatrix} \end{aligned} \tag{2}$$

Manuscript received July 24, 2005; revised January 31, 2006.

V. G. Daniele is with the Dipartimento di Elettronica, Politecnico di Torino, 10129 Torino, Italy, and also with the Istituto Superiore Mario Boella, 10138 Torino, Italy (e-mail: vito.daniele@polito.it).

G. Lombardi is with the Dipartimento di Elettronica, Politecnico di Torino, 10129 Torino, Italy (email: guido.lombardi@polito.it).

Digital Object Identifier 10.1109/TAP.2006.880723

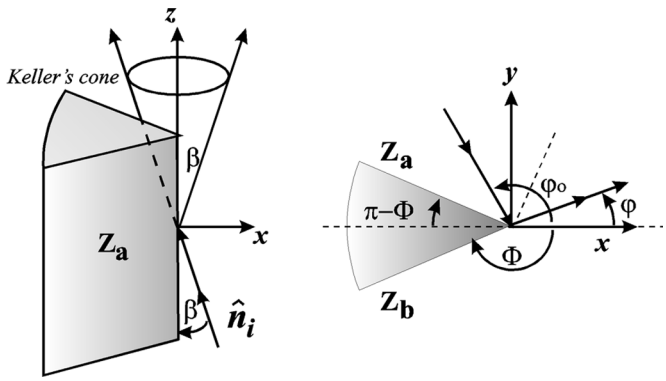

Fig. 1. The impenetrable wedge at skew incidence.

where $Z_o = \sqrt{\mu_o/\varepsilon_o}$ is the free-space impedance and the matrices $\mathbf{Z_{a,b}} = Z_o \begin{bmatrix} z_{11}^{a,b} & z_{12}^{a,b} \\ z_{21}^{a,b} & z_{22}^{a,b} \end{bmatrix}$ are the surface impedances which depend on the wedge material, in general anisotropic.

The well-known Sommerfeld–Malyuzhinets (SM) method [1]–[5] is a powerful procedure to solve exactly several special problems involving impenetrable wedges. This method is based on the solution of difference equations in the spectral domain. The SM has produced such an impressive number of important works that it is impossible to cite them extensively in a journal paper (see, for example [3], [5], and [6]). Recently, many authors have extended the SM method to deal with more cases relative to special problems [3]–[21] but the general solution of the wedge problem at skew incidence is not available using this technique. Several authors have proposed efficient approximate solutions for the unsolved problems [3]–[5], [22]–[31]. Even if relevant progress has been carried out, no general unified method has been proposed to solve the wedge diffraction at skew incidence.

An alternative and popular technique for solving particular wedge problems is based on the Wiener–Hopf (W-H) technique [32]–[36] but the use of this technique has been limited to deal only with rectangular geometries up to now.

In the last five years, a general theory based on the Wiener–Hopf technique has been developed to study electromagnetic problems in arbitrary angular regions [37]–[41]. In general, this technique yields a new class of functional equations called generalized Wiener-Hopf equations (GWHEs). The GWHEs differ from the classical Wiener-Hopf equations (CWHEs) [32]–[34] since the plus and minus functions of GWHE are defined into two or more different complex planes. It is important that for impenetrable wedges, a suitable mapping reduces the GWHEs to the classical ones.

The aim of this paper is to apply the W-H technique to solve the general diffraction problem of the impenetrable wedge at skew incidence efficiently. We have found closed-form W-H solutions by using an explicit factorization of the matrix kernels not only for problems that have been studied with SM method [37], [38], but also for problems studied with other methods. For problems where no closed-form W-H factorization is available, we obtain optimal approximate solutions by using Fredholm equations of second kind derived directly from the W-H factorization problem. We observe also that in the framework of the SM method, approximate techniques are obtained by reducing difference equations to the Fredholm integral equation [4], [28], [29]. The main difference is that the W-H equations yield directly the Fredholm integral equation of the second kind, avoiding the necessity of a regularization process. In particular, in the W-H approach, the kernel of the Fredholm equation does not involve special functions such as Malyuzhinets's and can be evaluated immediately by algebraic consideration of the geometrical problem.

This paper is organized as follows. Section II reports the Wiener–Hopf formulation of the problem without the mathematical details of [37]–[41] but from an applied point of view, Section III introduces and solves the Fredholm equation relevant to the W-H equations. Section IV presents the efficiency and the convergence of the approximate solution through a comparison with exact solution of some canonical problems. Section V presents the far-field evaluation for arbitrary impenetrable wedges at skew incidence and Section VI reports the conclusions. Two important appendixes are included in this paper. The first is a theoretical appendix devoted to explaining the mapping between the complex planes used in this paper. The second is a tool for applications by engineers: we present in a systematic way the evaluation of the far-field from the Wiener–Hopf solution by applying GTD and UTD.

II. W-H Formulation

A. Generalized W-H Equations for Impenetrable Wedge Problems

The Wiener–Hopf technique for wedge problems, defined in [37], is based on the introduction of the following Laplace transforms in the η complex plane:

$$V_{z+}(\eta,\varphi)=\int_0^\infty E_z(\rho,\varphi)e^{j\eta\rho}d\rho$$
$$I_{z+}(\eta,\varphi)=\int_0^\infty H_z(\rho,\varphi)e^{j\eta\rho}d\rho \tag{3}$$
$$V_{\rho+}(\eta,\varphi)=\int_0^\infty E_\rho(\rho,\varphi)e^{j\eta\rho}d\rho$$
$$I_{\rho+}(\eta,\varphi)=\int_0^\infty H_\rho(\rho,\varphi)e^{j\eta\rho}d\rho \tag{4}$$

where the subscript $+$ corresponds to plus functions, i.e., regular functions in the upper half-plane of the η-plane. According to the theory presented in [37], the GWHE for the impenetrable wedge problem assumes the following form [41]:

$$G(\eta)X_+(\eta)=X_-(m) \tag{5}$$

where $G(\eta)=D^{-1}(m)S(\eta)$ and with

$$X_+(\eta)=\begin{vmatrix} V_{z+}(\eta,0)\\ V_{\rho+}(\eta,0)\\ Z_oI_{z+}(\eta,0)\\ Z_oI_{\rho+}(\eta,0)\end{vmatrix},\quad X_-(m)=\begin{vmatrix} Z_oI_{\rho+}(-m,\Phi)\\ -Z_oI_{z+}(-m,\Phi)\\ -Z_oI_{\rho+}(-m,-\Phi)\\ Z_oI_{z+}(-m,-\Phi)\end{vmatrix} \tag{6}$$

$$S(\eta)=\begin{vmatrix} \xi & 0 & -\frac{\alpha_o\eta}{k} & -\frac{\tau_o^2}{k}\\ \frac{\alpha_o\eta}{k} & \frac{\tau_o^2}{k} & \xi & 0\\ \xi & 0 & \frac{\alpha_o\eta}{k} & \frac{\tau_o^2}{k}\\ -\frac{\alpha_o\eta}{k} & -\frac{\tau_o^2}{k} & \xi & 0\end{vmatrix}. \tag{7}$$

$D(m)$ is reported in (9), shown at the bottom of the page. The previous quantities are defined in terms of

$$\begin{cases}\xi=\sqrt{\tau_o^2-\eta^2}\\ m=-\eta\cos\Phi+\xi\sin\Phi\\ n=-\eta\sin\Phi-\xi\cos\Phi\end{cases}. \tag{8}$$

Note that, in the expression $\xi=\sqrt{\tau_o^2-\eta^2}$, we define the proper branch of the square root as the one that assumes the value τ_o for $\eta=0$. See (9).

B. Reduction of GWHE to CWHE

In order to solve GWHE (5), let us introduce the special mapping defined by [37], [38]

$$\eta=\eta(\bar\eta)=-\tau_o\cos\left(\frac{\Phi}{\pi}\arccos\left(-\frac{\bar\eta}{\tau_o}\right)\right). \tag{10}$$

Applying this mapping, we obtain

$$m=m(\bar\eta)=\tau_o\cos\left(\frac{\Phi}{\pi}\arccos\left(-\frac{\bar\eta}{\tau_o}\right)+\Phi\right)$$

and then (5) becomes

$$\bar G(\bar\eta)\bar X_+(\bar\eta)=\bar X_-(\bar\eta) \tag{11}$$

$$D(m)=\begin{vmatrix} -nz_{11}^a-\frac{\tau_o^2}{k} & -nz_{12}^a-\frac{m\alpha_o}{k} & 0 & 0\\ -\frac{mz_{11}^a\alpha_o}{k}+\frac{z_{21}^a\tau_o^2}{k} & n-\frac{mz_{12}^a\alpha_o}{k}+\frac{z_{22}^a\tau_o^2}{k} & 0 & 0\\ 0 & 0 & -nz_{11}^b-\frac{\tau_o^2}{k} & -nz_{12}^b-\frac{m\alpha_o}{k}\\ 0 & 0 & \frac{mz_{11}^b\alpha_o}{k}-\frac{z_{21}^b\tau_o^2}{k} & -n+\frac{mz_{12}^b\alpha_o}{k}-\frac{z_{22}^b\tau_o^2}{k}\end{vmatrix} \tag{9}$$

where $\bar{G}(\bar{\eta}) = G(\eta(\bar{\eta}))$, $\bar{X}_+(\bar{\eta}) = X_+(\eta(\bar{\eta}))$, and $\bar{X}_-(\bar{\eta}) = X_-(m(\bar{\eta}))$.

A complete study of mapping (10) is described in [37] and [38]. Note that (11) is now a classical W-H equation [32]–[34] in the $\bar{\eta}$-plane that is solvable by the standard factorization procedure for matrix kernels

$$\bar{G}(\bar{\eta}) = \bar{G}_-(\bar{\eta})\bar{G}_+(\bar{\eta}). \tag{12}$$

C. Formal Solution of the W-H Equations for Wedge Problems

As the standard Wiener–Hopf procedure needs to extract from the unknowns the known term, we introduce the source term in (11). The source term is the geometrical optics component of the field due to the plane waves defined by $\varphi_r = (-1)^r\varphi_o + 2r\Phi$, $r\epsilon\mathbb{N}$. All possible plane waves assume the same pole in the multisheet $\bar{\eta}$-plane [38]

$$\bar{\eta}_r = \bar{\eta}_o = -\tau_o \cos\frac{\pi}{\Phi}\varphi_o. \tag{13}$$

The incident field is related to the plus function $\bar{X}_+(\bar{\eta})$ for $r = 0$ and provides the pole $\bar{\eta}_o$ that is located in the proper sheet of the $\bar{\eta}$-plane. To obtain the source term in the W-H equations (11), we start from the incident field $X_+^i(\eta)$ that is present in $X_+(\eta)$

$$X_+^i(\eta) = \frac{T_o}{\eta + \tau_o\cos\varphi_o} \tag{14}$$

where

$$T_o = \begin{vmatrix} jE_o \\ j\frac{\alpha_o\cos\varphi_o E_o + kZ_o\sin\varphi_o H_o}{\tau_o} \\ jZ_oH_o \\ j\frac{\alpha_o Z_o\cos\varphi_o H_o - k\sin\varphi_o E_o}{\tau_o} \end{vmatrix}. \tag{15}$$

T_o are the coefficients of the incident field according to the definition of $X_+(\eta)$. By applying mapping (10), we obtain the source term in the $\bar{\eta}$-plane

$$\bar{X}_+^o(\bar{\eta}) = \frac{\bar{T}_o}{\bar{\eta} - \bar{\eta}_o}$$

where

$$\bar{T}_o = T_o\left.\frac{d\bar{\eta}}{d\eta}\right|_{\bar{\eta}=\bar{\eta}_o} = T_o\frac{\pi}{\Phi}\frac{\sin\frac{\pi}{\Phi}\varphi_o}{\sin\varphi_o}. \tag{16}$$

Using the decomposition procedure, we obtain

$$\bar{X}_+(\bar{\eta}) = \bar{X}_+^s(\bar{\eta}) + \bar{X}_+^o(\bar{\eta}) \tag{17}$$

where $\bar{X}_+^s(\bar{\eta})$ is the unknown and $\bar{X}_+^o(\bar{\eta})$ is the incident field in $\bar{\eta}$-plane.

Taking into account (17), the W-H technique applied to (11) yields the solution [32], [39]

$$\begin{aligned}\bar{X}_+(\bar{\eta}) &= \bar{G}_+^{-1}(\bar{\eta})\bar{G}_+(\bar{\eta}_o)\frac{\bar{T}_o}{\bar{\eta} - \bar{\eta}_o} \\ \bar{X}_-(\bar{\eta}) &= \bar{G}_-(\bar{\eta})\bar{G}_+(\bar{\eta}_o)\frac{\bar{T}_o}{\bar{\eta} - \bar{\eta}_o}.\end{aligned} \tag{18}$$

D. The Electromagnetic Field in the Wedge Problem

The W-H solution (18) provides the Laplace transforms of the electromagnetic fields only along the directions $\varphi = 0, \pm\Phi$; see (6) and (11).

Using the equivalence theorem or the functional equations reported in [38], it is possible to obtain the expression for the field's components for any φ value: $V_{z+}(\eta,\varphi)$, $V_{\rho+}(\eta,\varphi)$, $I_{z+}(\eta,\varphi)$, $I_{\rho+}(\eta,\varphi)$. Therefore, in general, there is no need to introduce the Sommerfeld functions $s_E(w)$ and $s_H(w)$ in order to obtain the field components in the physical domain.

However, in this paper, we follow the standard procedure used in the current literature. See, for example, [3] and [42]. We define the Sommerfeld functions in terms of the W-H solution (plus functions for $\varphi = 0$).

The $s_E(w)$ and $s_H(w)$ are given by (20) [43], where the w-plane is defined by

$$\eta = -\tau_o\cos w \tag{19}$$

and (20) as shown at the bottom of the page.

The longitudinal components of field are obtained through the following expressions for any φ value:

$$\begin{aligned}E_z(\rho,\varphi) &= \frac{1}{2\pi j}\left[\int_\gamma s_E(w+\varphi)e^{+j\tau_o\cos(w)\rho}dw\right] \\ H_z(\rho,\varphi) &= \frac{1}{2\pi j}\left[\int_\gamma s_H(w+\varphi)e^{+j\tau_o\cos(w)\rho}dw\right].\end{aligned} \tag{21}$$

γ is the Sommerfeld contour; see, for example, [8]. Using the w-plane (see Appendix I), the parameter ξ, m, and n assume the following simple forms:

$$\xi = -\tau_o\sin w, \quad m = \tau_o\cos(w+\Phi), \quad n = \tau_o\sin(w+\Phi).$$

$$\begin{aligned}s_E(w) &= \frac{j}{2}\left[-\tau_o\sin w V_{z+}(-\tau_o\cos w, 0) + \frac{\tau_o^2}{\omega\varepsilon}I_{\rho+}(-\tau_o\cos w, 0) - \frac{\alpha_o\tau_o\cos w}{\omega\varepsilon}I_{z+}(-\tau_o\cos w, 0)\right] \\ s_H(w) &= \frac{j}{2}\left[-\tau_o\sin w I_{z+}(-\tau_o\cos w, 0) - \frac{\tau_o^2}{\omega\mu}V_{\rho+}(-\tau_o\cos w, 0) + \frac{\alpha_o\tau_o\cos w}{\omega\mu}V_{z+}(-\tau_o\cos w, 0)\right]\end{aligned} \tag{20}$$

In the following we will use also the $\bar{w}$-plane defined in (53) and the following notations for quantities defined in different spectral domains:

$$f(\eta) = f(-\tau_o \cos w) = \hat{f}(w) = \bar{f}(\bar{\eta}) = \bar{f}(-\tau_o \cos \bar{w}) = \tilde{f}(\bar{w}). \tag{22}$$

Equation (20) provides the Sommerfeld functions only for $w \in P_w$ that corresponds to the proper sheet of the $\bar{\eta}$-plane; see Appendix I. Conversely, (21) requires the Sommerfeld function in the whole w-plane. We extend the validity of (20) through analytical continuation. The analytical continuation is immediate when closed-form analytical solution $X_+(\eta) = \bar{X}_+(\bar{\eta}) = \hat{X}_+(w)$ is available, on the other hand it becomes a critical operation when the unknown $\bar{X}_+(\bar{\eta})$ is given by approximate expressions which holds only in the proper sheet of the $\bar{w}$-plane; see Appendix I and Section II-E and III-C.

E. Analytical Continuation in the w-Plane

We recall from [37] that in the w-plane, the plus functions are even functions

$$\hat{X}_+(w) = \hat{X}_+(-w). \tag{23}$$

Besides in the whole w-plane, the W-H equation (5) assumes the following form:

$$\hat{G}(w)\hat{X}_+(w) = \hat{Y}_+(-w - \Phi) \tag{24}$$

where $Y_+(-m) = X_-(m)$ and (22) is applied. Considering (23), it is possible to remove the unknown $\hat{Y}_+(w)$ from (24) and it holds

$$\hat{X}_+(\pm w) = \hat{G}^{-1}(\mp w)\hat{G}(\pm w - 2\Phi)\hat{X}_+(\pm w - 2\Phi) \tag{25}$$

where

$$\hat{X}_+(w) = -\hat{G}_+^{-1}(w)\hat{G}_+(w_o)\frac{\bar{T}_o}{\tau_o \cos\left(\frac{\pi}{\Phi}w\right) - \tau_o \cos\left(\frac{\pi}{\Phi}\varphi_o\right)} \tag{26}$$

which holds for $w \in P_w$ and where $w_o = -|\varphi_o|$; see Appendix I.

By applying (23) and (25) to (26), we obtain the $\hat{X}_+(w)$ for any w value outside the P_w region.

F. Exact and Approximate Factorization of Matrix Kernels

The W-H technique applied to wedge problem constitutes a novel method that is completely different from the one known in the literature as the Sommerfeld–Malyuzhinets method. A comparison between the two methods shows that SM requires the solution of difference equations; instead the Wiener–Hopf technique involves decomposition and factorization.

We claim that all closed-form solutions for wedge problems (also the ones that have been recently published) reduce to matrix kernels that can be factorized in closed form [38].

However, for the general problem, no explicit factorization seems to be possible. Consequently, an approximate solution technique seems to be necessary. One of the aims of this paper is to show that for the wedge problem, approximate technique of factorization is reliable and efficient. There are procedures to obtain approximate factorizations of the W-H kernels [39]–[41]. For instance, it is possible to solve the factorization problem by introducing approximate rational representation of the matrix kernel of an arbitrary W-H equation [44] because it is possible to factorize rational matrices in closed form as reported in [39]. We have tested this technique for impenetrable wedge problems and we have obtained acceptable accuracy.

In this paper, we develop another technique to obtain approximate factorizations of matrix kernels. This technique is described in Section III and provides highly accurate results and good convergence, and it is quite simple to manage.

From an applied point of view, it is convenient to refer to the Appendix II, which provides expressions for the total uniform far-field for any observation angle φ: explicit expressions for the reflection coefficients for the general wedge problems, the use of UTD in Wiener–Hopf context, the analysis of the location of the structural singularities, and thus the surface-wave pole contributions.

III. Approximate Solutions of the W-H Equations

A. Factorized Matrices as Solutions of the Homogeneous Wiener–Hopf Problem

In order to factorize the matrix kernels, we consider the solution of the following homogeneous Wiener–Hopf problem with algebraic behavior as $\bar{\eta} \to \infty$:

$$\bar{G}(\bar{\eta})U_{i+}(\bar{\eta}) = U_{i-}(\bar{\eta}) \tag{27}$$

where the plus function $U_{i+}(\bar{\eta})$ and the minus function $U_{i-}(\bar{\eta})$ are respectively regular in the half-planes $\mathrm{Im}[\bar{\eta}] \geq 0$ and $\mathrm{Im}[\bar{\eta}] \leq 0$. We can define the factorized matrices of $\bar{G}(\bar{\eta}) = \bar{G}_-(\bar{\eta})\bar{G}_+(\bar{\eta})$ in term of four independent solutions $\{U_{i+}(\alpha), U_{i-}(\alpha)\}$, $\{i = 1, 2, 3, 4\}$ of (27) [39], [45]

$$\begin{aligned} \bar{G}_-(\bar{\eta}) &= |U_{1-}(\bar{\eta}), U_{2-}(\bar{\eta}), U_{3-}(\bar{\eta}), U_{4-}(\bar{\eta})| \\ \bar{G}_+(\bar{\eta}) &= |U_{1+}(\bar{\eta}), U_{2+}(\bar{\eta}), U_{2+}(\bar{\eta}), U_{4+}(\bar{\eta})|^{-1}. \end{aligned} \tag{28}$$

B. The Fredholm Equation for the Plus Function Defined in the $\bar{\eta}$-Plane

To obtain $U_{i+}(\bar{\eta})$, let us introduce the functions $\{i = 1, 2, 3, 4\}$

$$X_{i+}(\bar{\eta}) = \frac{U_{i+}(\bar{\eta})}{\bar{\eta} - \bar{\eta}_p} \tag{29}$$

where $\bar{\eta}_p$ is an arbitrary point with negative imaginary part. Equation (27) becomes

$$\bar{G}(\bar{\eta})X_{i+}(\bar{\eta}) = \frac{U_{i-}(\bar{\eta})}{\bar{\eta} - \bar{\eta}_p} \tag{30}$$

whose members vanish as $\bar{\eta} \to \infty$ according to the physical behavior of the matrix kernel $\bar{G}(\bar{\eta})$, the unknowns $X_{i+}(\bar{\eta})$, and $U_{i-}(\bar{\eta})/(\bar{\eta} - \bar{\eta}_p)$. By considering the procedure presented in

[45] and [39], we obtain the following integral equation for $X_{i+}(\bar{\eta})$, $\{i = 1, 2, 3, 4\}$:

$$\bar{G}(\bar{\eta})X_{i+}(\bar{\eta}) + \frac{1}{2\pi j}\int_{-\infty}^{\infty} \frac{\left[\bar{G}(x) - \bar{G}(\bar{\eta})\right] X_{i+}(x)}{x - \bar{\eta}} dx = \frac{R_i}{\bar{\eta} - \bar{\eta}_p} \tag{31}$$

with $\mathrm{Im}[\bar{\eta}_p] < 0$, and where the vector constant R_i are arbitrary: for example, the canonical basis for the $4D$ space. From (31), we obtain four independent solutions $X_{i+}(\bar{\eta})$.

These solutions provide the factorized matrix $\bar{G}_+(\bar{\eta})$ through (28) and (29). Equation (31) can be reduced to a Fredholm integral equation of second kind after a suitable reformulation of the unknown vector $X_{i+}(\bar{\eta})$. In fact, the kernel of the reformulated equation satisfies the compactness property [38], [39], [46]. In brief, the compactness of the kernel in (31) can be observed by taking into account that (with the exception of the cases where $z_{11}^a = 0$ and $z_{11}^b = 0$) all the components of the matrix $\bar{G}(\bar{\eta})$ are constants and bounded as $\bar{\eta} \to \infty$.

Different choices of $\bar{\eta}_p$ yield solutions of (31) (in terms of $\bar{G}_+(\bar{\eta})$) which are different by a premultiplicative constant matrix [39]. Thus the form of the solution (18) is not modified.

We suggest to define the pole $\bar{\eta}_p$ in the context of the physical problem: for the problem under examination, a suitable choice is the pole related to a physical source constituted by a plane wave.

C. Approximate Factorization in the $\bar{w}$-Plane

We found that the best way to provide approximate factorized matrices in wedge problems is to reformulate the Fredholm equation (31) in the $\bar{w}$-plane; see Appendix I. It is convenient to warp the contour path constituted by the real axis into the straight line λ_α that joins the points $j\tau_o$ and $-j\tau_o$ in order to obtain good convergence using numerical quadrature techniques [39], [47]. This warping yields (32) if no poles of $\bar{G}(\bar{\eta})$ are present in the region of the proper sheet between real axis and λ_α. We are not able to provide a mathematical proof that for arbitrary values of the wedge impedances, there are no poles in this region. However, using several different values of the matrices $\mathbf{Z_a}$ and $\mathbf{Z_b}$, we have verified numerically that no poles are in the specified region

$$H(t)Y_i(t) + \frac{1}{2\pi j}\int_{-\infty}^{+\infty} M(t,u)Y_i(u)du = \frac{-R_i}{\tau_o(j\sinh t - \cos\bar{w}_p)} \tag{32}$$

where the t (and u) variable is defined by $\bar{w} = -(\pi/2) + jt$; $\bar{\eta}_p = -\tau_o \cos\bar{w}_p$, $H(t) = \tilde{G}(-(\pi/2) + jt) = \tilde{G}(\bar{w})$, $Y_i(t) = \tilde{X}_{i+}(-(\pi/2) + jt) = \tilde{X}_{i+}(\bar{w})$, and

$$M(t,u) = \begin{cases} \lim\limits_{u\to t} \frac{[H(u)-H(t)]\cosh u}{-\sinh u + \sinh t} & u = t \\ \frac{[H(u)-H(t)]\cosh u}{-\sinh u + \sinh t} & u \neq t \end{cases}. \tag{33}$$

The sampled form of the previous Fredholm equation is

$$H(hr)Y_{ia}(hr) + \frac{h}{2\pi j}\sum_{s=-\frac{A}{h}}^{\frac{A}{h}} M(hr, hi)Y_{ia}(hs) = \frac{-R_i}{\tau_o(j\sinh hr - \cos\bar{w}_p)} \tag{34}$$

where $r = 0, \pm1, \pm2, \ldots, \pm(A/h)$, h has to be chosen as small as possible and A is to be chosen as large as possible. The solution of the previous equations for the $(2A/h)+1$ unknowns $Y_{ia}(hs)$ $(s = 0, \pm1, \pm2, \ldots, \pm(A/h))$ yields the following approximate representation of the elements $U_{i+}(\bar{\eta}) = \hat{U}_{i+}(w) \approx \hat{U}_{ia+}(w)$ of the factorized kernel $\hat{G}_+(w) = \bar{G}_+(\bar{\eta})$:

$$\hat{U}_{ia+}(w) = \hat{G}(w)^{-1} \cdot \left(R_i - \frac{(\bar{\eta} - \bar{\eta}_p)h}{2\pi j} \cdot \sum_{s=-\frac{A}{h}}^{\frac{A}{h}} M\left(-j\left(\frac{\pi}{\Phi}w + \frac{\pi}{2}\right), hs\right) Y_{ia}(hs) \right) \tag{35}$$

where $\bar{\eta} = -\tau_o \cos((\pi/\Phi)w)$; see Appendix I.

This representation is valid only in the P_w region; see Appendix I. We extend the validity of (35) through analytical continuation as described in Section II-E. In general, $\hat{U}_{i+}(w)$ is regular in the strip $-\Phi < \mathrm{Re}[w] < 0$ for impenetrable wedge problems. We extend this property in the strip $-\Phi < \mathrm{Re}[w] < \Phi$ with the property $\hat{U}_{ia+}(w) = \hat{U}_{ia+}(-w)$, because plus functions are even function in w. By using (25)

$$\hat{U}_{i+}(\pm w) = \hat{G}^{-1}(\mp w)\hat{G}(\pm w - 2\Phi)\hat{U}_{i+}(\pm w - 2\Phi) \tag{36}$$

we obtain $\hat{U}_{i+}(w)$ for any w value.

From (36), (35), (28), (26), and (20), we obtain the Sommerfeld functions in the interval $-3\Phi < \mathrm{Re}[w] < 3\Phi$ that are needed for far-field evaluation (Appendix II). Considering that the Fredholm solution gives directly correct evaluation of $\hat{X}_+(w)$ for $-\Phi \leq \mathrm{Re}[w] \leq 0$, we define

$$\hat{X}_+(w) = \begin{cases} \hat{X}_+(-w) & -3\Phi < \mathrm{Re}[w] < -\Phi \\ \hat{X}_+(w) & -\Phi \leq \mathrm{Re}[w] \leq 0 \\ \hat{X}_+(-w) & 0 \leq \mathrm{Re}[w] \leq \Phi \\ \hat{G}^{-1}(-w)\hat{G}(w - 2\Phi) \cdot \hat{X}_+(w - 2\Phi) & \Phi < \mathrm{Re}[w] < 3\Phi \end{cases}. \tag{37}$$

Besides, we observe that by using a suitable normalization, the factorized matrices in impenetrable wedge problems are independent on k.

IV. Comparison With Known Results and Validation

The efficiency, convergence, and validation of the approximate solutions found by using the technique of Sections II and III are illustrated through comparisons between exact and approximate solutions of several canonical problems. The quantities used in this section and in Section V are explicitly defined in Appendix II: field components, GTD diffraction coefficient, UTD field, and surface wave contributions.

A. Solution of the Symmetric Wedge at Normal Incidence

In the case of $\alpha_o = 0$ (normal incidence) and symmetric wedges (same isotropic impedance on the faces Z_a), the system of four coupled W-H equations reduces to four uncoupled scalar W-H equations. For the E-polarization ($H_{zo} = 0$), we have $E_{\rho+}(\rho,\varphi) = 0$, $H_{z+}(\rho,\varphi) = 0$, and we need to solve the two scalar W-H equations

$$\begin{cases} \frac{\xi}{n+n_a} V_{z+}(\eta,0) = \frac{Z_a}{2}\left[I_{\rho+}(-m,-\Phi) - I_{\rho+}(-m,\Phi)\right] \\ \frac{n_a}{n+n_a} I_{\rho+}(\eta,0) = \frac{1}{2}\left[I_{\rho+}(-m,-\Phi) + I_{\rho+}(-m,\Phi)\right] \end{cases} \tag{38}$$

where $Z_a = Z_o z_a$ is the impedance of the wedge and $n_a = \omega\mu/Z_a = k\sin\vartheta_a$. The factorization of the scalar kernels

$$\bar{g}_1(\bar{\eta}) = \frac{\xi}{n+n_a} = -\frac{\sin w}{\sin(w+\Phi)+\sin\vartheta_a} \tag{39}$$

$$\bar{g}_2(\bar{\eta}) = \frac{n_a}{n+n_a} = \frac{\sin\vartheta_a}{\sin(w+\Phi)+\sin\vartheta_a} \tag{40}$$

in the $\bar{\eta}$-plane has been performed in [37]

$$\hat{g}_{1+}(w) = \frac{\sin w}{d_\Phi(w)\sin\frac{\pi}{\Phi}w}, \quad \hat{g}_{2+}(w) = \frac{1}{d_\Phi(w)\cos\frac{\pi}{2\Phi}w} \tag{41}$$

where the special function $d_\Phi(w)$ [37] is defined by

$$d_\Phi(w) = \exp\left[\frac{1}{\pi}\int_0^\infty \arctan\left(\frac{1}{z_a\sinh\left(\frac{\Phi u}{\pi}\right)}\right)\frac{\sinh u}{\cosh u+\cos w}du\right]. \tag{42}$$

From the plus factorized functions $\hat{g}_{1+}(w)$ and $\hat{g}_{2+}(w)$, we obtain the exact solutions according to (18)

$$\begin{cases} \hat{V}_{z+}(w,0) = -j\frac{\pi}{\Phi}\frac{\sin\frac{\pi}{\Phi}\varphi_o}{k\sin\varphi_o}\frac{\hat{g}_{1+}(-\varphi_o)}{\hat{g}_{1+}(w)}\frac{E_o}{\cos\left(\frac{\pi}{\Phi}w\right)-\cos\left(\frac{\pi}{\Phi}\varphi_o\right)} \\ \hat{I}_{\rho+}(w,0) = j\frac{\pi}{\Phi}\frac{\sin\frac{\pi}{\Phi}\varphi_o}{kZ_o}\frac{\hat{g}_{2+}(-\varphi_o)}{\hat{g}_{2+}(w)}\frac{E_o}{\cos\left(\frac{\pi}{\Phi}w\right)-\cos\left(\frac{\pi}{\Phi}\varphi_o\right)} \end{cases}. \tag{43}$$

Equation (43) is valid only in the P_w region. However, since they are exact expressions, the process of analytical continuations makes them hold for any w point. For instance, even though the point $w = \varphi_o$ does not belong to P_w, we know that $\hat{g}_{1,2+}(-\varphi_o) = \hat{g}_{1,2+}(\varphi_o)$.

Using (43) in (20) and taking into account the relationship of the special function $d_\Phi(w)$ with the Malyuzhinets function $\psi(w)$ [37], we obtain the well-known result ($s_H = 0$) and

$$s_E(w) = \frac{E_o}{n_\Phi}\frac{\cos(\varphi_o/n_\Phi)}{\sin(w/n_\Phi)-\sin(\varphi_o/n_\Phi)}\frac{\psi(w)}{\psi(\varphi_o)} \tag{44}$$

where $n_\Phi = 2\Phi/\pi$, $\psi(w)$ is the function defined by [3, (4.15)], and $\vartheta_+ = \vartheta_- = \vartheta_a$.

Approximate values of $\hat{u}_{1a+}(w) \approx \hat{u}_{1+}(w) = 1/\hat{g}_{1+}(w)$ and $\hat{u}_{2a+}(w) \approx \hat{u}_{2+}(w) = 1/\hat{g}_{2+}(w)$ can be obtained through the procedure described in Section III that is based on the numerical solution of the suitable Fredholm equation. Note that outside the P_w region, we must use analytical continuations of (35).

The accuracy of the approximate technique of factorization is realized by comparing the exact functions $\hat{g}_{1+}(w)$ and $\hat{g}_{2+}(w)$ with $\hat{g}_{1a+}(w) = 1/\hat{u}_{1a+}(w)$ and $\hat{g}_{2a+}(w) = 1/\hat{u}_{2a+}(w)$ obtained numerically from the solution of Fredholm equations. For illustrative purposes, without lack of generality, we present the comparison between $\hat{g}_{1+}(w)$ and $\hat{g}_{1a+}(w)$ obtained as the plus factorized function of

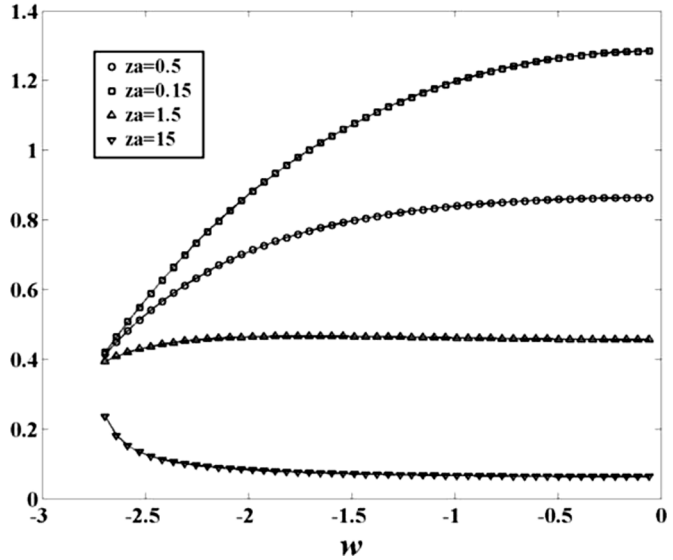

Fig. 2. The factorized functions $\hat{g}_{1+}(w)$ (solid line) and $\hat{g}_{1a+}(w)$ for the symmetric isotropic impedance wedge at normal incidence obtained, respectively, through (41) and the procedure described in Section III. The symbols refer to the numerical solution $\hat{g}_{1a+}(w)$ for different z_a values.

$$\hat{g}_1(w) = -\frac{k\sin w}{z_a\left(\sin(w+\Phi)+1/z_a\right)} \tag{45}$$

which differs from the previous definition of $\hat{g}_1(w)$ for an inessential constant. By assuming $A = 20$, $h = 0.5$, $\bar{w}_p = -6\pi/7$ (relative to a fictitious incident field at $\varphi_0 = 3\pi/4$) we solve the linear system (34) of $1\times((2A/h)+1)$ order for $\Phi = 7\pi/8$ and for the following four values of z_a: $z_a = 0.15, 0.5, 1.5, 15$.

In Fig. 2, plots of $\hat{g}_{1+}(w)$ (solid lines) and $\hat{g}_{1a+}(w)$ (symbols) are indistinguishable in the real range $-\Phi < w < 0$. Besides plots of the relative error in $\log_{10}$ scale

$$e(w) = \frac{|\hat{g}_{1+}(w) - \hat{g}_{1a+}(w)|}{|\hat{g}_{1+}(w)|} \tag{46}$$

in the real range $-\Phi < w < 0$ shows relatively small values; see Fig. 3.

The evaluation of $e(w)$ in the complex w plane yields the same size of error of those reported in the previous figures.

By using the procedure of Section II-C and the approximation of the plus factorized kernels, we obtain an approximate solution of the plus unknowns.

In addition to these results, in Fig. 4, we propose as validation the test case reported in [3, p. 122] by using our methodology. In particular, our reference system is referred to Fig. 1 and the test parameters are $k\rho = 10$ (where ρ is the radial distance from the edge of the wedge), the incident field $\varphi_o = 7\pi/12$, $E_o = 1$, $H_o = 0$, the aperture angle $\Phi = 3\pi/4$, the normalized face impedance $z_a = 0.5$, and the integration parameters $A = 10$, $h = 0.5$. Fig. 4 presents the decomposition of total field into

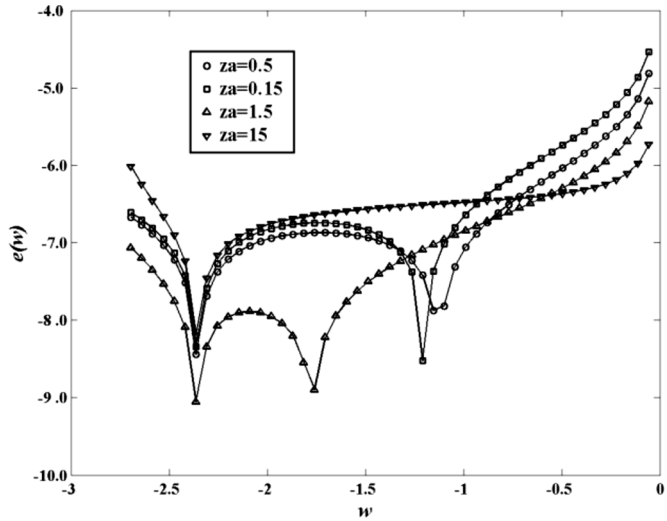

Fig. 3. The relative error $e(w)$ of the evaluation of the factorized function $\hat{g}_{1+}(w)$ in log_{10} scale; see Section IV-A. The symbols refer to different z_a values.

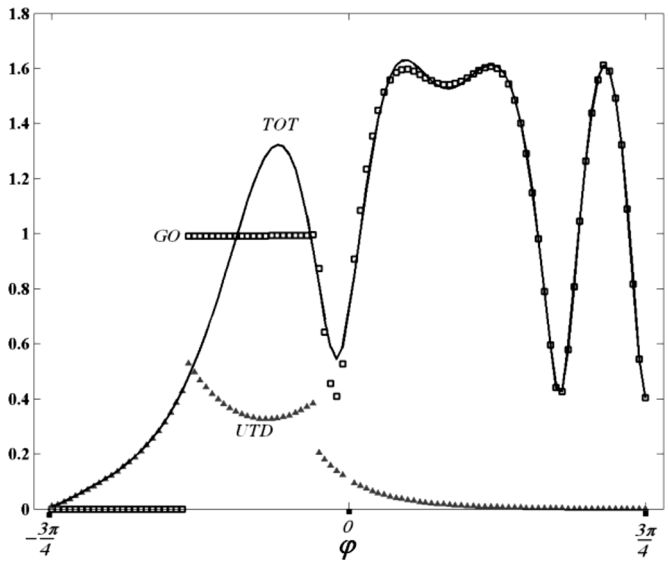

Fig. 4. Total field (solid line), GO field component (squares), and UTD field component (triangles) for $k\rho = 10$, $\varphi_o = 7\pi/12$, $E_o = 1$, $H_o = 0$, $\Phi = 3\pi/4$, $z_a = 0.5$, $A = 10$, $h = 0.5$; see Section IV-A.

two components: geometrical optics (GO) field component and UTD field component.

B. Solution of the Nonsymmetric Wedge at Normal Incidence With Surface Wave Contribution

In this section, we analyze another well-known test case reported in [42] using our methodology. Our reference system is referred to Fig. 1 and the test parameters are similar to the ones reported in the cited paper. In particular, we evaluate the total field H_z due to an H-polarized plane wave at $k\rho = 10$ from the edge of an impedance wedge with the following parameters: $E_o = 0$, $H_o = 1$, $\varphi_o = \pi/2$, $\Phi = 7\pi/8$, $z_a = 0.01$ (quasi-perfect conducting face), $z_b = \sin(\theta_b)$, $\theta_b = 0.01 + j$ (inductive impedance), $A = 10$, $h = 0.5$.

Fig. 5 presents the total field and its decomposition into three components: the GO field component, the UTD field component, and the surface wave (SW) field component.

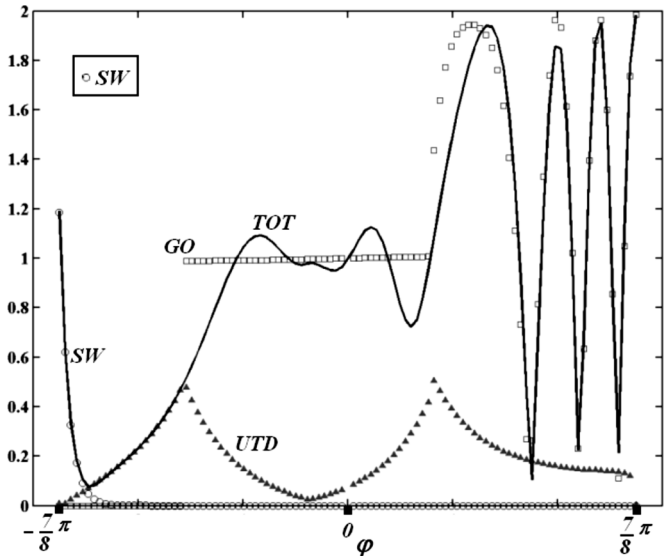

Fig. 5. Total field (solid line), GO field component (squares), UTD field component (triangles), and SW field component (circles) for $k\rho = 10$, $\varphi_o = \pi/2$, $E_o = 0$, $H_o = 1$, $\Phi = 7\pi/8$, $z_a = 0.01$, $z_b = \sin(\theta_b)$, $\theta_b = 0.01 + j$, $A = 10$, $h = 0.5$; see Section IV-B.

Note that the only difference from the test case reported in [42] is $z_a = 0.01$ instead of $z_a = 0$. This choice is made to check that our methodology does not have problems for some critical small values of the parameters. Similar results are obtained using $z_a = 0$.

C. Solution of a PEC Wedge at Skew Incidence

The factorization problem of the W-H kernel (11) related to the perfect electric conducting (PEC) wedge is reduced to the factorization in the $\bar{\eta}$-plane of the functions $\xi = \sqrt{\tau_o^2 - \eta^2}$ and $n = -\eta \sin\Phi - \xi\cos\Phi$; see [37]. From (11) and (26), we obtain the exact result (47) as shown at the bottom of the next page.

By using (20), we obtain the Sommerfeld functions

$$\begin{cases} s_E(w) = \pi \dfrac{E_o \cos\left(\frac{\pi}{2\Phi}\varphi_o\right)}{2\Phi\left[\sin\left(\frac{\pi}{2\Phi}w\right) - \sin\left(\frac{\pi}{2\Phi}\varphi_o\right)\right]} \\ s_H(w) = \pi \dfrac{H_o \cos\left(\frac{\pi}{2\Phi}w\right)}{2\Phi\left[\sin\left(\frac{\pi}{2\Phi}w\right) - \sin\left(\frac{\pi}{2\Phi}\varphi_o\right)\right]} \end{cases}. \tag{48}$$

Equation (48) agrees completely with the solutions obtained by the SM method [2], [3], [48].

The accuracy and the convergence of the approximate solutions can be ascertained by the comparison between the exact GTD diffraction coefficients (60) and the approximate ones obtained by the numerical solution of the linear system (34) of order $4\times((2A/h)+1)$.

With the analytical continuation (37) provided by (23) and (25), we obtain the Sommerfeld functions for any w point, in particular in the real range $-\Phi - \pi < w < \Phi + \pi$ to evaluate the diffracted field (59).

The test parameters are referred to Fig. 1 and to the definition presented previously: $\varphi_o = 2\pi/3$, $E_{zo} = 1$, $H_{zo} = 0$, $\Phi = 7\pi/8$, and the skew incidence $\beta = \pi/4$. For the numerical solution, we have chosen different values of the integration parameter A and h in order to confirm the convergence of our technique: $A = 5, 10, 20, 25$ and $h = 1, 0.5, 0.25$.

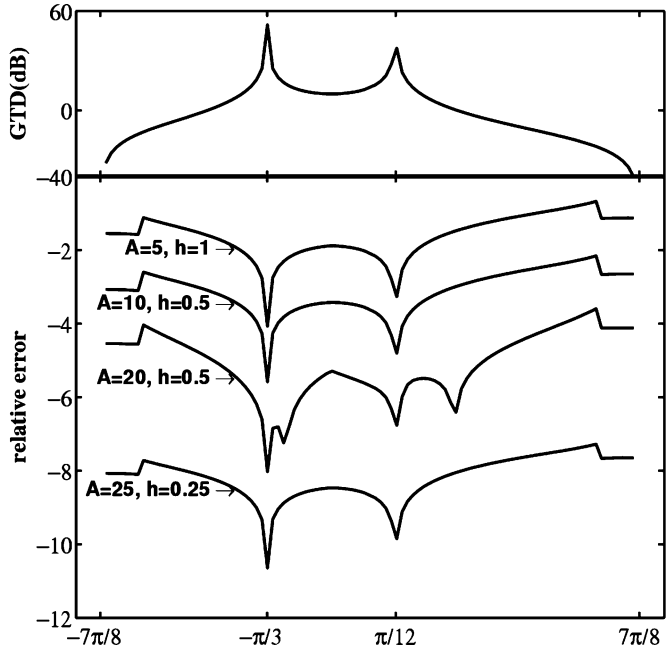

Fig. 6. The relative error of the evaluation of GTD diffraction coefficient in $\log_{10}$ scale using different set of integration parameters for the PEC wedge with $\varphi_o = 2\pi/3$, $E_{zo} = 1$, $H_{zo} = 0$, $\Phi = 7\pi/8$, and $\beta = \pi/4$ versus the azimuthal angle φ; see Section IV-C. The top portion of the figure reports the GTD diffraction coefficient (dB).

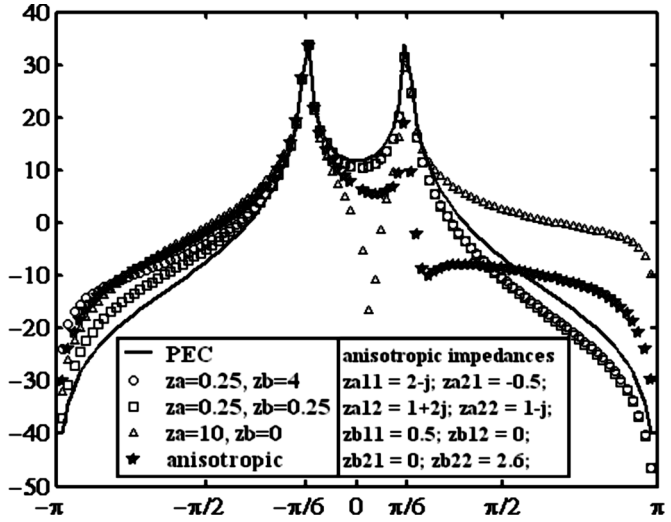

Fig. 7. GTD copolar diffraction coefficient (dB) versus the azimuthal angle φ for different sets of surface impedances for the half-plane problem; see Section V-A.

The exact GTD diffraction coefficient (in decibels) together with the relative error of the numerical solution in $\log_{10}$ scale is reported in Fig. 6. The use of the relative error (49) is a good tool to validate the precision because it measures the level of precision in term of digits ($\log_{10}$ scale) for the whole interval of the observation angle φ except for the directions where GTD is infinite or almost vanishing

$$e(\varphi) = \frac{\left|\tilde{D}(\varphi,\varphi_o) - D(\varphi,\varphi_o)\right|}{|D(\varphi,\varphi_o)|} \tag{49}$$

where $D(\varphi,\varphi_o)$ is the exact GTD coefficient (60), while $\tilde{D}(\varphi,\varphi_o)$ is the numerical estimation.

Peaks of the GTD diffraction coefficients occur for the GO directions: $\varphi = \varphi_o - \pi$ (incident field) and for $\varphi = 2\Phi - \varphi_o - \pi$ (reflected field).

Fig. 6 shows the relative error of $\leq 1/10\,000\,000$ for $A = 25$, $h = 0.25$ for any observation angle.

This high convergence rate is due to the mathematical properties of Fredholm integral equation of second kind obtained from GWHE without any regularization technique. Besides, for impenetrable wedge problems, the application of the contour path λ_α described in Section III-C enforces the convergence of the general kernel for wedge problems.

We have considered the PEC wedge at skew incidence, as a test case, to validate our general vector formulation with a well-known explicit scalar solution for GTD diffraction coefficient. We observe that even if the analytic expression of the GTD diffraction coefficients is independent of β, the W-H vector formulation depends on the value of β; see (47).

V. Solution of the Arbitrary Impenetrable Wedge at Skew Incidence

A. The Half-Plane Problem With Different Impedances at the Skew Incidence Case

In order to validate our method and demonstrate its convergence, we present the following test case partially reported in [3, p. 130]. This problem consists of the half-plane problem with different impedances at the skew incidence. Fig. 7 shows

$$\begin{aligned}
V_{z+}(-\tau_o\cos w,0) &= \hat{V}_{z+}(w,0) = 2j\pi\frac{E_o\cos\left(\frac{\pi}{2\Phi}\varphi_o\right)\sin\left(\frac{\pi}{2\Phi}\varphi_o\right)}{\tau_o\Phi\sin w\left[-\cos\left(\frac{\pi}{\Phi}w\right)+\cos\left(\frac{\pi}{\Phi}\varphi_o\right)\right]}\\
V_{\rho+}(-\tau_o\cos w,0) &= \hat{V}_{\rho+}(w,0) = j2\pi\frac{E_o\cos\left(\frac{\pi}{2\Phi}\varphi_o\right)\cot w\cot\beta\sin\left(\frac{\pi}{2\Phi}w\right)+Z_oH_o\cos\left(\frac{\pi}{2\Phi}w\right)\csc\beta\sin\left(\frac{\pi}{2\Phi}\varphi_o\right)}{\tau_o\Phi\left[-\cos\left(\frac{\pi}{\Phi}w\right)+\cos\left(\frac{\pi}{\Phi}\varphi_o\right)\right]}\\
I_{z+}(-\tau_o\cos w,0) &= \hat{I}_{z+}(w,0) = j\pi\frac{H_o\sin\left(\frac{\pi}{\Phi}w\right)}{\tau_o\Phi\sin w\left[-\cos\left(\frac{\pi}{\Phi}w\right)+\cos\left(\frac{\pi}{\Phi}\varphi_o\right)\right]}\\
I_{\rho+}(-\tau_o\cos w,0) &= \hat{I}_{\rho+}(w,0) = j\pi\frac{-Z_oH_o\cot w\cot\beta\sin\left(\frac{\pi}{\Phi}w\right)+E_o\csc\beta\sin\left(\frac{\pi}{\Phi}\varphi_o\right)}{Z_o\tau_o\Phi\left[\cos\left(\frac{\pi}{\Phi}w\right)-\cos\left(\frac{\pi}{\Phi}\varphi_o\right)\right]}
\end{aligned} \tag{47}$$

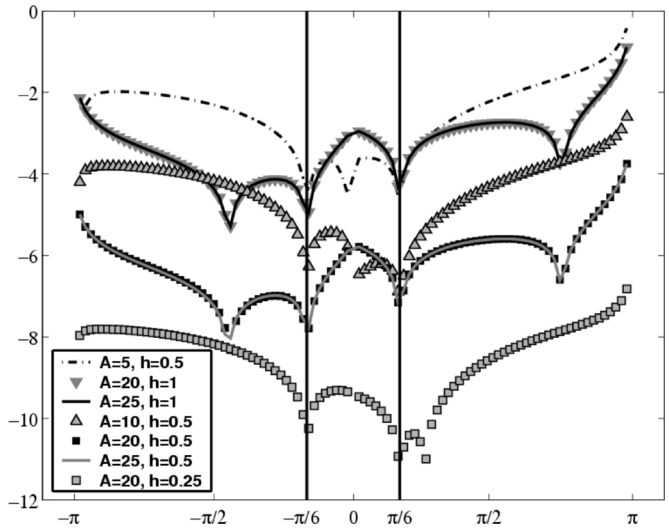

Fig. 8. The relative error on the evaluation of GTD diffraction coefficient in $\log_{10}$ scale using different set of integration parameters for the test case reported in Fig. 7 with $z_a = 0.25$, $z_b = 4$ (half-plane problem; see Section V-A).

the GTD copolar diffraction coefficient (dB) for the field component E_z versus the azimuthal angle φ with different sets of z_a and z_b scalar impedances (same as in [3]) and for an extra anisotropic case. The other problem's parameters are $\varphi_o = 5\pi/6$, $E_{zo} = 1$, $H_{zo} = 0$, $\Phi = \pi$ and $\beta = \pi/3$, $A = 10$, $h = 1$. The fifth test cases differ on the face impedances:

1) isotropic face impedances $z_a = 0$, $z_b = 0$ (PEC);
2) isotropic face impedances $z_a = 0.25$, $z_b = 4$;
3) isotropic face impedances $z_a = 0.25$, $z_b = 0.25$;
4) isotropic face impedances $z_a = 10$, $z_b = 0$;
5) anisotropic face impedances

$$\mathbf{z_a} = \begin{bmatrix} 2-j & 1+2j \\ -0.5 & 1-j \end{bmatrix}, \quad \mathbf{z_b} = \begin{bmatrix} 0.5 & 0 \\ 0 & 2.6 \end{bmatrix}. \tag{50}$$

Note that for the anisotropic test case, we have chosen passive impedance matrices.

In Fig. 8, the study of convergence using a particular case of the problems analyzed in Fig. 7 is proposed: $z_a = 0.25$, $z_b = 4$. This figure reports the relative error (49) of the GTD diffraction coefficient $\tilde{D}(\varphi, \varphi_o)$ in $\log_{10}$ scale for different integration parameters (A, h) and, considering as reference case $D(\varphi, \varphi_o)$, the solution for $A = 25$, $h = 0.25$.

It is useful to study the relative error because it measures the digits of precision in the numerical evaluation for different integration parameters (A, h). This measure is not possible in Fig. 7, where the standard decibel scale is used.

We observe that the parameter A selects the spectral range that we consider in the discretization of the $M(t, u)$ kernel [47]. From Fig. 8, we establish that a satisfactory choice of A is $A \geq 10$. In particular, for values over 20, no improvement of the solution is achieved. Small values of the parameter h improve the average level of convergence (digit of precision), especially for small GTD diffraction coefficients. A satisfactory choice of h is $h \leq 0.5$. In particular, for values below 0.25, no improvement of the solution is achieved—in fact, we have experienced that result for $A = 20$, $h = 0.1$ are indistinguishable from those with $A = 20$, $h = 0.25$.

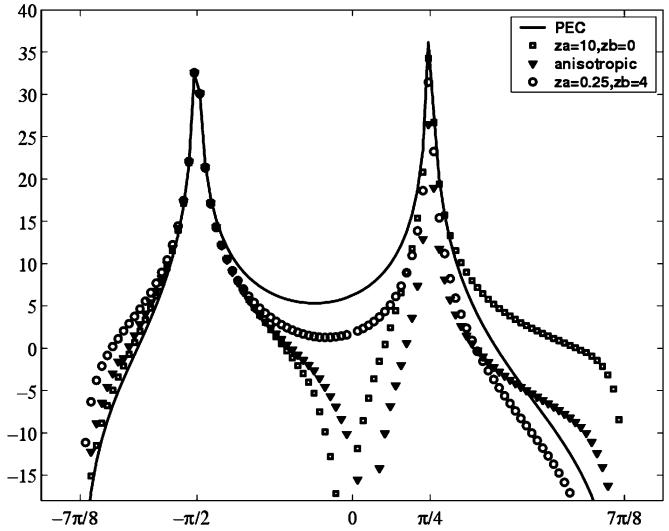

Fig. 9. GTD copolar diffraction coefficient (dB) versus the azimuthal angle φ for the wedge problem with $\Phi = 7\pi/8$ described in Section V-B.

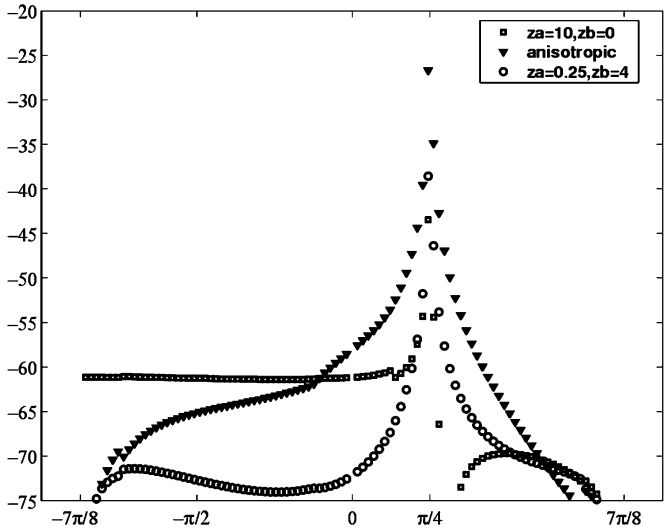

Fig. 10. GTD crosspolar diffraction coefficient (dB) versus the azimuthal angle φ for the wedge problem with $\Phi = 7\pi/8$ described in Section V-B.

Similar convergence properties are observed for the other test case of Fig. 7, in particular for the anisotropic case.

This high convergence rate is due to the mathematical properties of Fredholm integral equation of second kind and in particular to the spectral properties of its kernel in the t-plane; see Section III-C and [47].

B. The GTD Coefficients for an Arbitrary Impenetrable Wedge at Skew Incidence

Following the procedure presented in Sections II and III, we present the numerical results for the arbitrary impenetrable wedge at skew incidence. Figs. 9 and 10 present comparisons among the GTD diffraction coefficients for four different test cases with the following common parameters: $\varphi_o = \pi/2$, $E_{zo} = 1$, $H_{zo} = 0$, $\Phi = 7\pi/8$, $\beta = \pi/3$, $A = 10$, and $h = 0.5$. The four test cases differ in the face impedances. The impedance values are those reported in Section V-A, but for the sake of simplicity we avoid plotting the case $z_a = 0.25$, $z_b = 0.25$.

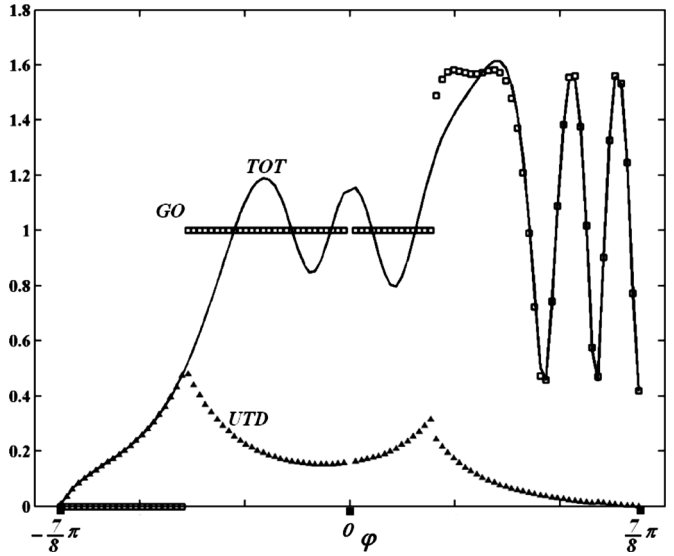

Fig. 11. Copolar component E_z of total field for the test case described in Section V-C for the wedge problem with $\Phi = 7\pi/8$: total field (solid line), GO field component (squares), UTD field component (triangles).

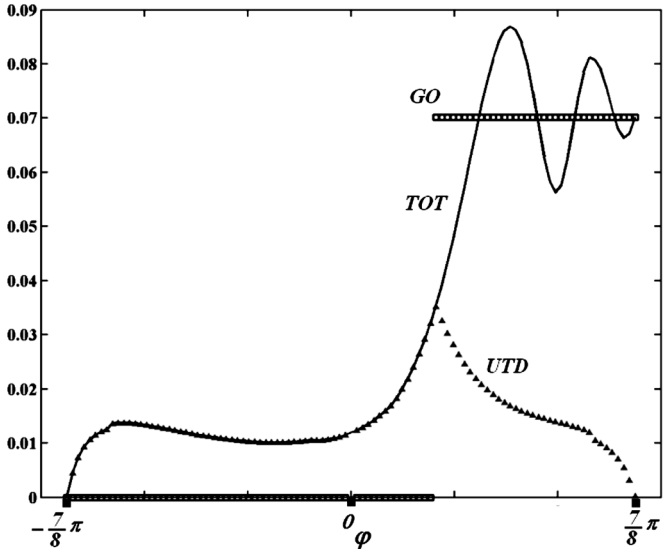

Fig. 12. Crosspolar component $Z_o H_z$ of total field for the test case described in Section V-C for the wedge problem with $\Phi = 7\pi/8$: total field (solid line), GO field component (squares), UTD field component (triangles).

Fig. 9 shows the GTD copolar diffraction coefficient (we observe E_z with an E_{zo} incident field). Fig. 10 shows the crosspolar diffraction coefficient (we observe H_z with an E_{zo} incident field). For practical engineering applications, we recall the relation (61) among E_z, H_z components and the E_β, E_φ components. Peaks of the GTD diffraction coefficients are for $\varphi = \varphi_o - \pi$ (incident field) and for $\varphi = 2\Phi - \varphi_o - \pi$ (reflected field).

C. Total Field for an Arbitrary Impenetrable Wedge at Skew Incidence

Here we present numerical results for the evaluation of the total field scattered and diffracted by a nonsymmetric isotropic impenetrable wedge. We evaluate the total E_z and $Z_o H_z$ components according to the description in Appendix II. We have chosen the following parameters: $\varphi_o = \pi/2$, $E_{zo} = 1$, $H_{zo} = 0$, $\Phi = 7\pi/8$, $\beta = \pi/3$, $z_a = 0.25$, $z_b = 4$, $A = 10$, and $h = 0.5$. Numerical results of the total field are reported in Fig. 11 (copolar component E_z) and Fig. 12 (crosspolar component H_z) specifying the GO field component and UTD field component.

VI. Conclusions

The GWHE formulation constitutes a new tool to solve wedge problems. Analytical details are presented in order to apply this novel technique to practical problems. Simple quadrature schemes are sufficient to demonstrate very good convergence of numerical results. The procedure to obtain diffraction coefficients and total fields for an anisotropic nonsymmetric wedge at skew incident is presented and fully tested.

Appendix I
The w and $\bar{w}$ Planes

In order to apply the analytical continuation in the w-plane to $\hat{X}_+(w) = X_+(\eta) = \bar{X}_+(\bar{\eta})$, a full analysis of mapping between w-plane and $\bar{\eta}$-plane is considered. By introducing the following mapping:

$$\bar{\eta} = -\tau_o \cos \bar{w} \tag{51}$$

we obtain that the points of $\bar{\eta}$ proper-sheet correspond to the $\bar{w}$ points through (52) [39]

$$\bar{w}(\bar{\eta}) = \begin{cases} -j \log\left(\frac{\bar{\eta}+j\kappa}{\tau_o}\right) - \pi & \arg\frac{\bar{\eta}+j\kappa}{\tau_o} > -\frac{\pi}{2} \\ -j \log\left(\frac{\bar{\eta}+j\kappa}{\tau_o}\right) + \pi & \arg\frac{\bar{\eta}+j\kappa}{\tau_o} \le -\frac{\pi}{2} \end{cases}. \tag{52}$$

In (52), the proper branch of $\kappa = \sqrt{\tau_o^2 - \bar{\eta}^2}$ and the principal value of $\log(z)$ assume that $\mathrm{Im}[\kappa] \le 0$, $\log(z) = \log|z| + j\arg(z)$ with $-\pi < \arg(z) \le +\pi$.

Fig. 13 shows the image of the proper sheet of the $\bar{\eta}$-plane onto the $\bar{w}$-plane. The images of four quadrants are limited by the images of the standard branch lines labelled with $b_{-\bar{w}}$ and $b_{+\bar{w}}$. We assume as standard branch lines of the mapping (51) those constituted by the arcs of hyperbolas where $\mathrm{Im}[\kappa] = 0$; see Fig. 14. The line $r_{\bar{w}}$ and $i_{\bar{w}}$ of Fig. 13 is, respectively, the image of the real and imaginary axis of the $\bar{\eta}$-plane.

Using (10), (19), (51), and (52) we obtain that

$$w = \frac{\Phi}{\pi}\bar{w}. \tag{53}$$

We assume that P_w is the image of the proper $\bar{\eta}$-plane in the w-plane. $\bar{w}$ real values of the $\bar{\eta}$ proper sheet are those in the range $-\pi < \bar{w} < 0$ (52) and correspond to w real values of the interval $-\Phi < w < 0$ of P_w.

For instance, point w_o, which corresponds to the pole $-\tau_o \cos((\pi/\Phi)\varphi_o)$ and is located in the proper sheet of the $\bar{\eta}$-plane, is given by

$$w_o = -|\varphi_o|. \tag{54}$$

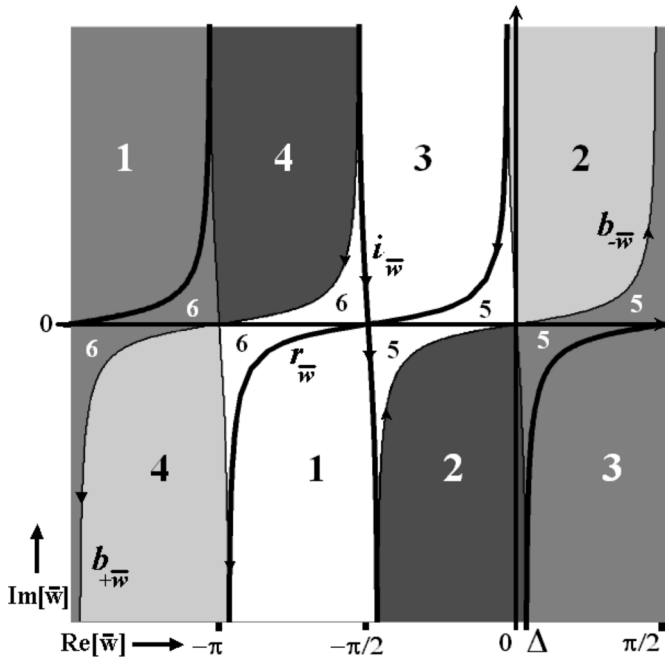

Fig. 13. This plot shows the image of the proper sheet and improper sheet of the $\bar{\eta}$-plane onto the $\bar{w}$-plane, respectively, with light gray colors and dark gray colors. For the proper sheet, the images of four quadrants 1, 2, 3, and 4 are limited by the images of the standard branch lines labelled with $b_{-\bar{w}}$ and $b_{+\bar{w}}$. The $r_{\bar{w}}$ and $i_{\bar{w}}$ lines are the images of the real and imaginary axes of the $\bar{\eta}$-plane. Regions 5 and 6 are, respectively, part of the second and fourth quadrant of $\bar{\eta}$-plane but with different κ properties: real and imaginary parts of κ for regions 5 and 6 are with the same sign of those relative to the first and third quadrant. Δ is $\arctan[-\mathrm{Im}[\tau_o]/\mathrm{Re}[\tau_o]]$. In the figure, τ_o is equal to $1-j0.1$.

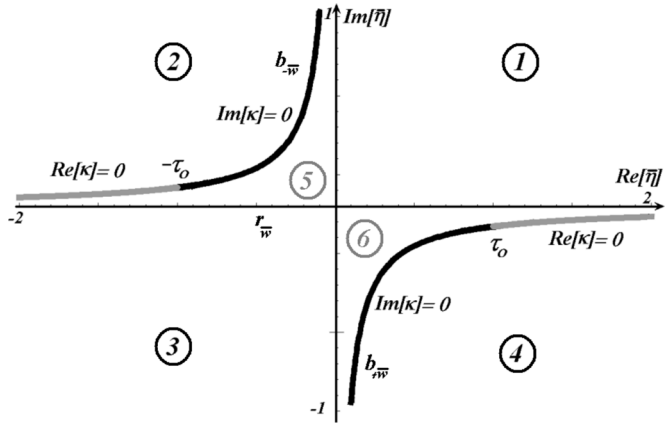

Fig. 14. Proper sheet of the $\bar{\eta}$-plane with four quadrants 1, 2, 3, and 4 limited by the images of the standard branch lines labelled with $b_{-\bar{w}}$ and $b_{+\bar{w}}$. Regions 5 and 6 are, respectively, part of the second and fourth quadrants of $\bar{\eta}$-plane but with different κ properties: real and imaginary parts of κ for regions 5 and 6 are with the same sign of those relative to the first and third quadrant. In the figure, τ_o is equal to $1-j0.1$.

By using $\eta = -\tau_o \cos w$, $\bar{\eta} = -\tau_o \cos \bar{w}$, and $\bar{w} = (\pi/\Phi)w$ we obtain the analytical continuation in the whole w and $\bar{w}$ planes for the following fundamental quantities:

$$\begin{aligned} \xi &= -\tau_o \sin w, \quad \kappa = -\tau_o \sin \bar{w}, \\ m &= \tau_o \cos(w+\Phi), \quad n = \tau_o \sin(w+\Phi). \end{aligned} \tag{55}$$

Appendix II
Far-Field Evaluation

In this Appendix, we propose from an applied point of view the immediate expressions for the total uniform far-field for any observation angle φ in a systematic way: explicit expressions of the reflection coefficients for the general wedge problems, the use of UTD in Wiener–Hopf solution context, the analysis of the location of the structural singularities, and thus surface-wave pole contributions.

In order to evaluate the field's components in impenetrable wedge problems for any observation point (ρ, φ), we apply (37) to the solution $X_+(\eta)$, which depends on the factorized kernel $\bar{G}_\pm(\bar{\eta})$. The use of the saddle point method (SDP) on (21) [3], [42] yields the far-field evaluation

$$\begin{aligned} E_z(\rho,\varphi) &= E_z^g(\rho,\varphi) + E_z^d(\rho,\varphi) + E_z^s(\rho,\varphi) \\ H_z(\rho,\varphi) &= H_z^g(\rho,\varphi) + H_z^d(\rho,\varphi) + H_z^s(\rho,\varphi) \end{aligned} \tag{56}$$

where E_z^g, H_z^g are the GO contributions, E_z^d, H_z^d the diffracted fields, and E_z^s, H_z^s the possible contributions of the surface waves. In the following, we assume without lack of generality only acute wedges: $\Phi > \pi/2$. The contribution of geometrical optics field arises from the residues of the poles w_r that satisfy the equation $\cos((\pi/\Phi)w_r) - \cos((\pi/\Phi)\varphi_o) = 0$ and that are present in $\prod^{\mathrm{RES}}$ [42] (the region enclosed by the SDP in $\pm\pi$ and the Sommerfeld contour γ). GO field can be evaluated by solving the simple problems of reflection of plane waves on flat indefinite impedance surfaces

$$\begin{aligned} E_z^g = e^{-j\alpha_o z} \Big[& E_o u(\pi - |\varphi - \varphi_o|)\, e^{j\tau_o \rho \cos(\varphi-\varphi_o)} \\ & + u(\pi - |\varphi + \varphi_o - 2\Phi|) \\ & \cdot R_a^E(\Phi - \varphi_o) e^{j\tau_o\rho\cos(\varphi+\varphi_o-2\Phi)} \\ & + u(\pi - |\varphi + \varphi_o + 2\Phi|) \\ & \cdot R_b^E(\Phi + \varphi_o) e^{j\tau_o\rho\cos(\varphi+\varphi_o+2\Phi)} \Big] \\ H_z^g = e^{-j\alpha_o z} \Big[& H_o u(\pi - |\varphi - \varphi_o|)\, e^{j\tau_o \rho \cos(\varphi-\varphi_o)} \\ & + u(\pi - |\varphi + \varphi_o - 2\Phi|) \\ & \cdot R_a^H(\Phi - \varphi_o) e^{j\tau_o\rho\cos(\varphi+\varphi_o-2\Phi)} \\ & + u(\pi - |\varphi + \varphi_o + 2\Phi|) \\ & \cdot R_b^H(\Phi + \varphi_o) e^{j\tau_o\rho\cos(\varphi+\varphi_o+2\Phi)} \Big] \end{aligned} \tag{57}$$

where $u(x)$ is the unit step function and $R_{a,b}^{E,H}(\chi)$ is related to the reflection coefficient for a skew plane wave incident on a flat impedance surface with $\mathbf{Z_{a,b}} = Z_o \begin{bmatrix} z_{11}^{a,b} & z_{12}^{a,b} \\ z_{21}^{a,b} & z_{22}^{a,b} \end{bmatrix}$. $R_{a,b}^{E,H}(\chi)$ is defined as

$$\begin{aligned} R_a^E(\chi) &= \frac{R_a^{EE}(\chi)E_o + R_a^{EH}(\chi)H_o}{den(\chi)}; \\ R_a^H(\chi) &= \frac{R_a^{HE}(\chi)E_o + R_a^{HH}(\chi)H_o}{Z_o den(\chi)} \end{aligned}$$

in terms of the coefficients reported in (58) as shown at the bottom of the next page.

The reflection coefficients of the b face (R_b^E and R_b^H) are the same as those of the a face after substituting z_{ij}^a with z_{ij}^b, Ho with $-Ho$ and Eo with $-Eo$.

The diffracted field components arise from the saddle points in $w = \pm\pi$ and present the following form [3], [42], known in the literature as the GTD component:

$$E_z^d(\rho,\varphi,z) = e^{-j\alpha_o z}\frac{e^{-j\left(\tau_o\rho+\frac{\pi}{4}\right)}}{\sqrt{2\pi\tau_o\rho}}\left[s_E(\varphi-\pi)-s_E(\varphi+\pi)\right]$$
$$H_z^d(\rho,\varphi,z) = e^{-j\alpha_o z}\frac{e^{-j\left(\tau_o\rho+\frac{\pi}{4}\right)}}{\sqrt{2\pi\tau_o\rho}}\left[s_H(\varphi-\pi)-s_H(\varphi+\pi)\right]. \tag{59}$$

We define as GTD diffraction coefficients

$$D^E(\varphi,\varphi_o) = s_E(\varphi-\pi)-s_E(\varphi+\pi)$$
$$D^H(\varphi,\varphi_o) = s_H(\varphi-\pi)-s_H(\varphi+\pi). \tag{60}$$

It is convenient to relate the transverse component E_β^d, E_φ^d of the diffracted ray to the transverse component E_β^i, E_φ^i of the incident ray [3]

$$E_\beta^d = -\frac{1}{\sin\beta}E_z^d, \quad E_\varphi^d = -\frac{1}{\sin\beta}Z_o H_z^d$$
$$E_z^i = \sin\beta E_\beta^i, \quad H_z^i = \frac{1}{Z_o}\sin\beta E_{\varphi_o}^i. \tag{61}$$

When the observation point approaches shadow boundaries, the GO poles are near the saddle points and uniform diffracted fields appear necessary. By using the UTD, we obtain [49]–[52]

$$E_z^d(\rho,\varphi,z) = e^{-j\alpha_o z}\frac{e^{-j\left(\tau_o\rho+\frac{\pi}{4}\right)}}{\sqrt{2\pi\tau_o\rho}}C^E(\varphi,\varphi_o)$$
$$H_z^d(\rho,\varphi,z) = e^{-j\alpha_o z}\frac{e^{-j\left(\tau_o\rho+\frac{\pi}{4}\right)}}{\sqrt{2\pi\tau_o\rho}}C^H(\varphi,\varphi_o) \tag{62}$$

where

$$C^{E,H}(\varphi,\varphi_o) = \left[s_{E,H}(\varphi-\pi)-s_{E,H}(\varphi+\pi)\right] + \frac{1-F\left(2\tau_o\rho\cos^2\frac{\varphi-\varphi_o}{2}\right)}{2\cos\frac{\varphi-\varphi_o}{2}} + R_a^{E,H}(\Phi-\varphi_o)\frac{1-F\left(2\tau_o\rho\cos^2\frac{\varphi+\varphi_o-2\Phi}{2}\right)}{2\cos\frac{\varphi+\varphi_o-2\Phi}{2}} + R_b^{E,H}(\Phi+\varphi_o)\frac{1-F\left(2\tau_o\rho\cos^2\frac{\varphi+\varphi_o+2\Phi}{2}\right)}{\cos\frac{\varphi+\varphi_o+2\Phi}{2}}$$

and the function $F(z)$ is the Kouyoumjian–Pathak transition function defined by [51]

$$F(z) = 2j\sqrt{z} \cdot\left[e^{jz}\int_{\sqrt{z}}^{\infty} e^{-js^2}ds - \sqrt{\pi}e^{j(z-\pi/4)}u\left(\arg\sqrt{z}-\frac{\pi}{4}\right)\right]. \tag{63}$$

In (63), the principal branch of $\sqrt{z}$ is the one for $-3\pi/4 < \arg\sqrt{z} < 5\pi/4$. The unit step function in $F(z)$ compensates the unit step function of the GO fields. Consequently, $E_z^g(\rho,\varphi,z)+E_z^d(\rho,\varphi,z)$ and $H_z^g(\rho,\varphi,z)+H_z^d(\rho,\varphi,z)$ are continuous when they cross the shadow boundaries. Note that (59) is based on the first-order saddle point approximation [53]. If the first-order contributions vanish, we must use complete asymptotic expansion as reported in [53]. The contributions of the surface waves arise from the structural poles and we discuss them next.

A. Structural Singularities and Surface-Wave Pole Contributions

The structural singularities of a W-H equation are defined by the singularities of the matrix kernel $G(\eta)$ and its inverse. In the GWHE (5) these matrices are defined by

$$G(\eta) = D^{-1}(m)S(\eta), \quad G^{-1}(\eta) = S^{-1}(\eta)D(m). \tag{64}$$

$$\begin{aligned}
R_a^{EE}(\chi) &= -\left(z_{11}^a\cos^2(\beta)\cos^2(\chi)\right) + (z_{12}^a+z_{21}^a)\cos(\beta)\cos(\chi)\sin(\beta) - z_{22}^a\sin^2(\beta)\\
&\quad + (-1+Det[Z_a])\sin(\beta)\sin(\chi) + z_{11}^a\sin^2(\chi)\\
R_a^{EH}(\chi) &= 2Z_o\left(z_{11}^a\cos(\beta)\cos(\chi) - z_{12}^a\sin(\beta)\right)\sin(\chi)\\
R_a^{HE}(\chi) &= 2\left(-z_{11}^a\cos(\beta)\cos(\chi) + z_{21}^a\sin(\beta)\right)\sin(\chi)\\
R_a^{HH}(\chi) &= Z_o\left(-\left(z_{11}^a\cos^2(\beta)\cos^2(\chi)\right) + (z_{12}^a+z_{21}^a)\cos(\beta)\cos(\chi)\sin(\beta) - z_{22}^a\sin^2(\beta)\right.\\
&\quad \left. - (-1+Det[Z_a])\sin(\beta)\sin(\chi) + z_{11}^a\sin^2(\chi)\right)\\
den(\chi) &= z_{11}^a\cos^2(\beta)\cos^2(\chi) - (z_{12}^a+z_{21}^a)\cos(\beta)\cos(\chi)\sin(\beta) + z_{22}^a\sin^2(\beta)\\
&\quad + (1+Det[Z_a])\sin(\beta)\sin(\chi) + z_{11}^a\sin^2(\chi)
\end{aligned} \tag{58}$$

We observe the presence of the branch points $\pm\tau_o$. In addition, since both $D(m)$ and $S(\eta)$ do not have poles, the structural singularities are the poles that arise from the zeroes of $Det[D(m)]$ and $Det[S(\eta)]$

$$Det\left[S(\eta)\right] = -\frac{4\left(\tau_o^2-\eta^2\right)\tau_o^4}{k^2}$$
$$Det\left[D(m)\right] = -\frac{\tau_o^4}{k^4}d_a(m)d_b(m) \tag{65}$$

where

$$d_\sigma(m) = \left(n^2+\alpha_o^2\right)z_{11}^\sigma + kn\left(1+Det[\mathbf{Z}_\sigma]\right) - m\alpha_o\left(z_{12}^\sigma+z_{21}^\sigma\right)+\tau_o^2 z_{22}^\sigma$$

with $\sigma = a, b$.

Note that the zeros of $Det[S(\eta)]$ are $\pm\tau_o$. Since they are also branch points of the matrix kernel $G(\eta)$, they do not add structural singularities. Conversely, $Det[D(m)]$ presents zeros defined by $d_a(m)=0$ and $d_b(m)=0$. These zeros are related to the possible complex waves present, respectively, on the a-face and on the b-face. According to (21), these poles may play a role in the far-field evaluation. It is possible to perform the analytical evaluation of the poles with the substitution $m=\tau_o\cos\psi$. It yields

$$\hat{d}_{a,b}(\psi) = \left(\tau_o^2\sin^2\psi+\alpha_o^2\right)z_{11}^{a,b} + k\tau_o\sin\psi\left(1+Det[\mathbf{Z_{a,b}}]\right) - \alpha_o\tau_o\cos\psi\left(z_{12}^{a,b}+z_{21}^{a,b}\right)+\tau_o^2 z_{22}^{a,b}.$$

By applying the residue theorem, we obtain

$$E_z^s(\rho,\varphi,z) = \sum_i \mathrm{Res}\left[s_E(w+\varphi)\right]_{w=w_i} e^{+j\tau_o\cos w_i\rho}e^{-j\alpha_o z}$$
$$H_z^s(\rho,\varphi,z) = \sum_i \mathrm{Res}\left[s_H(w+\varphi)\right]_{w=w_i} e^{+j\tau_o\cos w_i\rho}e^{-j\alpha_o z} \tag{66}$$

where w_i are the structural poles of $s_{E,H}(w+\varphi)$ in Π^{RES}. From (37) and (55), these poles satisfy the equation $\hat{d}_{a,b}(\pm(w_i+\varphi)-\Phi)=0$.

Concerning the surface-wave contributions, we observe that the evaluation of the field near a face of an impedance wedge through (66) could present an insufficient accuracy [54], [55] under particular conditions: for example, when the surface poles approach the saddle points.

REFERENCES

[1] G. D. Malyuzhinets, "Excitation, reflection and emission of surface waves from a wedge with given face impedances," *Sov. Phys. Dokl.*, vol. 3, pp. 752–755, 1958.

[2] A. V. Osipov and A. N. Norris, "The Malyuzhinets theory for scattering from wedge boundaries: A review," *Wave Motion*, vol. 29, pp. 313–340, 1999.

[3] T. B. A. Senior and J. L. Volakis, *Approximate Boundary Conditions in Electromagnetics*. London, U.K.: Institution of Electrical Engineers, 1995.

[4] B. Budaev, *Diffraction by Wedges*. London, UK: Longman Scientific, 1995.

[5] V. S. Buldyrev and M. A. Lyalinov, *Mathematical Methods in Modern Diffraction Theory*. Tokyo, Japan: Science House, 2001.

[6] G. Pelosi and J. L. Volakis, Eds., "The centennial of Sommerfield's diffraction problem," *Electromagnetics (Special Issue)*, vol. 18, no. 3, May–Jun. 1998.

[7] J. M. L. Bernard, "Diffraction at skew incidence by an anisotropic impedance wedge in electromagnetism theory; A new class of canonical cases," *J. Phys. A: Math. Gen.*, vol. 31, no. 2, pp. 595–613, Jan. 1998.

[8] G. Pelosi, G. Manara, and P. Nepa, "Electromagnetic scattering by a wedge with anisotropic impedance faces," *IEEE Antennas Propag. Ma.*, vol. 40, pp. 29–35, Dec. 1998.

[9] M. A. Lyalinov and N. Y. Zhu, "Exact solution to diffraction problem by wedges with a class of anisotropic impedance faces: Oblique incidence of a plane electromagnetic wave," *IEEE Trans. Antennas Propag.*, vol. 51, pp. 1216–1220, Jun. 2003.

[10] G. Manara and P. Nepa, "Electromagnetic diffraction of an obliquely incident plane wave by a right-angled anisotropic impedance wedge with a perfectly conducting face," *IEEE Trans. Antennas Propag.*, vol. 48, pp. 547–565, Apr. 2000.

[11] G. Manara, P. Nepa, and G. Pelosi, "Skew incidence diffraction by an anisotropic impedance half plane with a PEC face and arbitrarily oriented anisotropy axes," *IEEE Trans. Antennas Propag.*, vol. 52, pp. 487–496, Feb. 2004.

[12] ——, "High-frequency EM scattering by edges in artificially hard and soft surfaces illuminated at oblique incidence," *IEEE Trans. Antennas Propag.*, vol. 48, pp. 790–800, May 2000.

[13] P. Nepa, G. Manara, and A. Armogida, "Electromagnetic scattering by anisotropic impedance half and full planes illuminated at oblique incidence," *IEEE Trans. Antennas Propag.*, vol. 49, pp. 106–108, Jan. 2001.

[14] Y. A. Antipov and V. V. Silvestrov, "Vector functional-difference equation in electromagnetic scattering," *IMA J. Appl. Math.*, no. 69, pp. 27–69, 2004.

[15] ——, "Second-order functional-difference equations—I: Method of the Riemann-Hilbert problem on Riemann surfaces," *Q. J. Mech. Appl. Math.*, vol. 57, no. 2, pp. 245–265, 2004.

[16] ——, "Second-order functional-difference equations—II: Scattering from a right-angled conductive wedge for E-polarization," *Q. J. Mech. Appl. Math.*, vol. 57, no. 2, pp. 267–313, 2004.

[17] C. Demetrescu, "A general solution of the second-order difference equation occurring in diffraction theory," *Radio Sci.*, no. 31, pp. 461–467, 1996.

[18] T. B. A. Senior and S. R. Legault, "Second-order difference equations in diffraction theory," *Radio Sci.*, no. 35, pp. 683–690, 2000.

[19] C. Demetrescu, C. C. Constantinou, and M. J. Mehler, "Diffraction by a right-angled resistive wedge," *Radio Sci.*, no. 33, pp. 39–53, 1998.

[20] S. R. Legault and T. B. A. Senior, "Solution of a second-order difference equation using the bilinear relations of Riemann," *J. Math. Phys.*, no. 43, pp. 1598–1621, 2002.

[21] C. Demetrescu, C. C. Constantinou, M. J. Mehler, and B. V. Budaev, "Diffraction by a resistive sheet attached to a two-sided impedance plane," *Electromagnetics*, no. 18, pp. 315–332, 1998.

[22] H. J. Bilow, "Scattering by an infinite wedge with tensor impedance boundary conditions—A moment method/physical optics solution for the currents," *IEEE Trans. Antennas Propag.*, vol. 39, pp. 767–773, Jun. 1991.

[23] G. Pelosi, G. Manara, and P. Nepa, "A UTD solution for the scattering by a wedge with anisotropic impedance faces: Skew incidence case," *IEEE Trans. Antennas Propag.*, vol. 46, no. 4, pp. 579–588, Apr. 1998.

[24] G. Pelosi, S. Selleri, and R. D. Graglia, "The parabolic equation model for the numerical analysis of the diffraction at an anisotropic impedance wedge," *IEEE Trans. Antennas Propag.*, vol. 45, no. 5, pp. 767–771, 1997.

[25] N. Y. Zhu and F. M. Landstofer, "Numerical study of diffraction and slope-diffraction at anisotropic impedance wedges by the method of parabolic equation: space waves," *IEEE Trans. Antennas Propag.*, vol. 45, pp. 822–828, 1997.

[26] A. V. Osipov, "A hybrid technique for the analysis of scattering by impedance wedges," in *Proc. URSI Int. Symp. Electromagn. Theory*, Pisa, Italy, 2004, vol. 2, pp. 1140–1142.

[27] B. V. Budaev and D. B. Bogy, "Two-dimensional diffraction by a wedge with impedance boundary conditions," *IEEE Trans. Antennas Propag.*, vol. 53, pp. 2073–2080, Jun. 2005.

[28] M. A. Lyalinov and N. Y. Zhu, "A solution procedure for second-order difference equations and its application to electromagnetic-wave diffraction in a wedge-shaped region," *Proc. Roy. Soc. Lond. A*, no. 459, pp. 3159–3180, 2003.

[29] N. Y. Zhu and M. A. Lyalinov, "Diffraction of a normally incident plane wave by an impedance wedge with its exterior bisected by a semi-infinite impedance sheet," *IEEE Trans. Antennas Propag.*, vol. 52, pp. 2753–2758, Oct. 2004.

[30] T. B. A. Senior and S. R. Legault, "Diffraction by an anisotropic impedance half plane at skew incidence," *Electromagnetics*, no. 18, pp. 207–225, 1998.

[31] T. B. A. Senior, S. R. Legault, and J. L. Volakis, "A novel technique for the solution of second-order difference equations," *IEEE Trans. Antennas Propag.*, vol. 49, pp. 1612–1617, Dec. 2001.

[32] B. Noble, *Methods Based on the Wiener-Hopf Technique: For the Solution of Partial Differential Equations*. London, U.K.: Pergamon, 1958.
[33] L. A. Weinstein, *The Theory of Diffraction and the Factorization Method: Generalized Wiener-Hopf Technique* Transl.: P. Beckmann. Boulder, CO: Golem, 1969.
[34] R. Mittra and S. W. Lee, *Analytical Techniques in the Theory of Guided Waves*. New York: MacMillan, 1971.
[35] T. B. A. Senior, "Some problems involving imperfect half plane," in *Electromagnetic Scattering*, P. L. E. Uslenghi, Ed. New York: Academic, 1978.
[36] R. A. Hurd and E. Luneburg, "Diffraction by an anisotropic impedance half plane," *Can. J. Phys.*, vol. 63, no. 9, pp. 1135–1140, Sep. 1985.
[37] V. Daniele, "The Wiener-Hopf technique for impenetrable wedges having arbitrary aperture angle," *SIAM J. Appl. Math.*, vol. 63, no. 4, pp. 1442–1460, 2003.
[38] ——, The Wiener-Hopf technique for wedge problems Dipartimento di Elettronica, Politecnico di Torino, Internal Rep. ELT-2004-2, Oct. 2004 [Online]. Available: http://www.eln.polito.it/staff/daniele/
[39] ——, An Introduction to the Wiener-Hopf Technique For The Solution Of Electromagnetic Problems Dipartimento di Elettronica, Politecnico di Torino, Internal Rep. ELT-2004-1, Sep. 2004 [Online]. Available: http://www.eln.polito.it/staff/daniele/
[40] V. Daniele and G. Lombardi, "Generalized Wiener-Hopf equations for wedge problems involving arbitrary linear media," in *Int. Conf. Electromagn. Adv. Applicat. (ICEAA03)*, Torino, Italy, Sep. 2003, pp. 761–764.
[41] V. G. Daniele and G. Lombardi, "The Wiener-Hopf technique for impenetrable wedge problems," in *Days on Diffraction 2005 Int. Conf.*, Saint Petersburg, Russia, Jun. 2005, pp. 50–61.
[42] A. N. Norris and A. V. Osipov, "Far field analysis of the Malyuzhinets solution for plane and surface waves diffraction by an impedance wedge," *Wave Motion*, vol. 30, pp. 69–89, 1999.
[43] V. G. Daniele, "Rotating waves in the Laplace domain for angular regions," *Electromagnetics*, vol. 23, no. 3, pp. 223–236, 2003.
[44] I. D. Abrahams, "On the non commutative factorization of Wiener-Hopf kernels of Khrapkov type," *Proc. Roy. Soc. London A*, vol. 454, pp. 1719–1743, 1998.
[45] N. P. Vekua, *Systems of Singular Integral Equations*. Groningen, The Netherlands: Noordhoff, 1967.
[46] D. Jones, *Methods in Electromagnetic Wave Propagation*. Oxford, U.K.: Clarendon, 1979.
[47] G. Lombardi, "Numerical validation of the Wiener-Hopf approach to wedge problems," in *Int. Conf. Electromagn. Adv. Applicat. (ICEAA05)*, Torino, Italy, Sep. 2005, pp. 693–696.
[48] J. J. Bowman, T. B. A. Senior, and P. L. E. Uslenghi, Eds., *Electromagnetic and Acoustic Scattering by Simple Shapes*. New York: Hemisphere, 1969.
[49] R. G. Kouyoumjian and P. H. Pathak, "A uniform geometrical theory of diffraction for an edge in a perfectly conducting surface," *Proc. IEEE*, vol. 62, pp. 1448–1461, Nov. 1974.
[50] R. Tiberio, G. Pelosi, G. Manara, and P. H. Pathak, "High-frequency scattering from a wedge with impedance faces illuminated by a line source, Part I: Diffraction," *IEEE Trans. Antennas Propag.*, vol. 37, pp. 212–218, Feb. 1989.
[51] R. G. Kouyoumjian, G. Manara, P. Nepa, and B. J. E. Taute, "The diffraction of an inhomogeneous plane wave by a wedge," *Radio Sci.*, vol. 31, no. 6, pp. 1387–1397, Nov.–Dec. 1996.
[52] G. Manara, R. Tiberio, G. Pelosi, and P. H. Pathak, "High-frequency scattering from a wedge with impedance faces illuminated by a line source, Part II: Surface waves," *IEEE Trans. Antennas Propag.*, vol. 41, pp. 877–883, Jul. 1993.
[53] L. B. Felsen and N. Marcuvitz, *Radiation and Scattering of Waves*. Englewood Cliffs, NJ: Prentice-Hall, 1973.
[54] A. Osipov, K. Hongo, and H. Kobayashi, "High-frequency approximations for electromagnetic field near a face of an impedance wedge," *IEEE Trans. Antennas Propag.*, vol. 50, pp. 930–940, Jul. 2002.
[55] Q. A. Naqvi, K. Hongo, and H. Kobayashi, "Surface fields of an impedance wedge at skew incidence," *Electromagnetics*, vol. 22, no. 3, pp. 209–233, 2002.

Vito G. Daniele was born in Catanzaro, Italy, on March 20, 1942. He received the degree in electronic engineering from Polytechnic of Turin, Italy, in 1966.

In 1980, he became a full Professor in electrical engineering at the University of Catania. Since 1981, he has been a Professor of electrical engineering at the Polytechnic of Turin. He has published more than 150 papers in refereed journals and conference proceedings and several textbook chapters. His research interests are mainly in analytical and approximate techniques for the evaluation of electromagnetic fields both in high and in low frequency. He was the Guest Editor of a special issue on "Electromagnetic Coupling to Transmission Lines" for *Electromagnetics* in 1988, Chairman and Invited Speaker for several international symposia, and Reviewer for many international journals. He has been a Consultant to various industries in Italy.

Guido Lombardi (S'02–M'04) was born in Florence, Italy, on December 8, 1974. He received the laurea degree *(summa cum laude)* in telecommunications engineering from the University of Florence, Italy, in 1999 and the Ph.D. degree in electronics engineering from the Polytechnic of Turin, Italy, in 2004.

In 2000–2001, he was an Officer in the Italian Air Force. In 2004, he was an Associate Researcher with the Department of Electronics, Polytechnic of Turin, and in 2005 he joined the same department as an Assistant Professor. He was a member of the Organizing Committee of the International Conference on Electromagnetics in Advanced Applications (ICEAA), Turin, Italy, for the 2001 and 2003 editions and as the ICEAA Scientific Secretariat for the 2005 edition. In 2003, he was a Research Visitor with the Department of Electrical and Computer Engineering, University of Houston, Houston, TX. His Ph.D. work was focused on the study of analytical and numerical aspects of electromagnetic singularities. His research areas comprise analytical and numerical methods for electromagnetics, Wiener–Hopf method, theoretical and computational aspects of finite-element method and method of moments, electromagnetic singularities, waveguide problems, microwave passive components, and orthomode transducers.

Dr. Lombardi received the Raj Mittra Travel Grant award, as Junior Researcher, at the 2003 IEEE AP-S International Symposium and USNC/CNC/URSI National Radio Science Meeting, Columbus, OH.